Soft Matter

PAPER

View Article Online
View Journal | View Issue

Cite this: *Soft Matter*, 2025, **21**, 5990

Molecular architecture modulates self-assembly and micellar rheology of model ionic surfactant systems†

Stephen L. Flores, ‡*[a] Christopher P. Cabry,‡[ad] Hugh Barlow,[b] Joseph Peterson,[c] Joanne L. Cook,[d] Olga Mihailova,[d] Ian P. Stott,[d] Carlos Avendaño *[a] and Christopher Hardacre *[a]

Understanding and predicting the rheology of micellar systems is key in formulation design with wide-reaching implications for the development of products such as shampoos and detergents. In micellar systems comprising ionic surfactants, predictive models are uniquely challenging to construct as a result of the combined effects of salt screening and surfactant polydispersity on micelle self-assembly. In this work, we provide critical insights into how the amphiphilic nature of ionic surfactants controls self-assembly and rheological behaviour. For pure sodium lauryl ether sulphate surfactants, we demonstrate that the properties of micellar solutions can be described from the average properties of the constituent ingredients. Furthermore, we show that there are three distinct viscosity regimes with varying salt concentrations, and that formulation/property relationships can be systematically controlled by three key aspects of the surfactant molecular geometry in relation to micelle self-assembly: (1) the size of the hydrophilic headgroup (degree of ethoxylation), (2) the length of the hydrocarbon tail, and (3) the polydispersity of the surfactant solutions. In systems with multiple headgroup lengths, the salt concentration required to reach peak viscosity depends exclusively on the average number of ethoxy linkers, while the peak viscosity varies with the relative proportions of the surfactant components. The observed Gaussian symmetry in viscosity trends underscores the intricate relationship between molecular structure and macroscopic behaviour in these systems. These findings have implications for improvements in rheological, thermodynamics, molecular, and predictive models and the design and development of novel formulations.

Received 11th March 2025,
Accepted 29th June 2025

DOI: 10.1039/d5sm00252d

rsc.li/soft-matter-journal

1. Introduction

Above a certain concentration, surfactants in aqueous solutions self-assemble into micelles providing value-added functionality for applications ranging from consumer products to advanced oil recovery.[1] Surfactants are amphiphiles composed of a hydrophilic head group and a hydrophobic tail, and in multi-phase systems they have a strong preference for adsorbing at oil–water and water–oil interfaces, modifying the chemical, mechanical, and electrostatic properties of the interface that allow them to modify fluid interfacial properties. Where no interfaces are present or where there is more surfactant than available surface area, surfactant molecules in bulk water can self-assemble into a range of shapes (spheres, ropes, sheets) depending on the detailed chemical and geometric properties of the surfactant molecules present in the system. These self-assembled structures will, in turn, alter the properties of the bulk material (*e.g.* viscosity) and are key to fine-tuning formulations of personal care products.

Sodium dodecyl sulphate (SDS) and sodium lauryl ether sulphate (SLE_nS) are widely used anionic surfactants in the formulation of shampoos, detergents[2,3] and emulsion,[4] as fracking agents,[5] and for nanoparticle synthesis.[6] They are sodium salts of alkyl sulphates characterised by a sulphated headgroup and a tail that comprises a hydrocarbon chain, with

[a] *Department of Chemical Engineering, School of Engineering, The University of Manchester, Oxford Rd., Manchester M13 9PL, UK. E-mail: stephen.flores@manchester.ac.uk, carlos.avendano@manchester.ac.uk, c.hardacre@manchester.ac.uk*
[b] *Unilever Safety and Environmental Assurance Centre, Sharnbrook, Bedford MK44 1LQ, UK*
[c] *Department of Chemical and Biomolecular Engineering, Samueli School of Engineering, University of California, Los Angeles, CA 90095, USA*
[d] *Unilever Research and Development Port Sunlight, Quarry Road East, Bebington CH63 3JW, UK*

† Electronic supplementary information (ESI) available. See DOI: https://doi.org/10.1039/d5sm00252d

‡ These authors contributed equally.

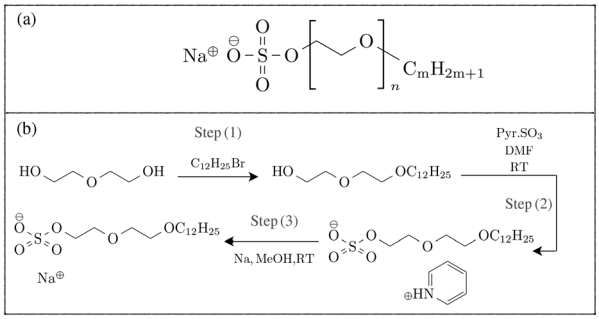

Fig. 1 (a) Chemical structure of the sodium alkyl ethoxy sulphate denoted as SC_mE_nS, where n is the degree of ethoxylation in the headgroup and m the alkyl chain length of the hydrocarbon tail. (b) 3-step synthetic route to form $SC_{12}E_2S$, also referred to as SLE_2S.

a general structure shown in Fig. 1(a). For convenience, these systems are denoted in this work as SC_mE_nS, where SLE_nS corresponds to the particular case with m = 12 and different degrees of ethoxylation n, while SDS corresponds to the case where m = 12 and n = 0. However, in industrial applications, these materials are intrinsically polydisperse, exhibiting variability in the number of ethoxy linkers n and the alkyl tail length m. This polydispersity introduces significant degrees of freedom related to these formulations (*e.g.*, mean, variance), and this makes material characterisation challenging.[7–9] For example, the viscosity of micellar solutions of SLE_nS tends to change with the degree of polydispersity,[10–12] and additives such as salt (NaCl)[2] are essential to ensure the viscosity of the final product remains in spec.[13]

SLE_nS is commercially produced from fatty alcohols that undergo ethoxylation, sulfonation, and subsequent neutralisation, leading to a product that contains a range of molecules with varying degrees of ethoxylation n and alkyl tail lengths m together with unreacted starting materials, intermediate materials, and components from side reactions.[13] When added to commercial products, these polydisperse solutions are usually characterised by a specification of active content (surfactant concentration), average degree of ethoxylation $\bar{n}$, average alkyl tail length $\bar{m}$, salt content and unsulphated alcohol content.

These surfactants are commonly used as base formulations for personal care products along with other co-surfactants because of the ease of modulating their flow properties with the addition of salt. Salt curves describe the bulk zero-shear viscosity of a surfactant solution as a function of the added salt content, reflecting changes in surfactant aggregation due to charge screening effects in solution.[2,13–15] The transition of the self-assembling units from spherical to wormlike, to branched micelles, and other complex structures can be observed implicitly through changes in the viscosity. At low concentrations, increasing salt favours larger worm-like aggregates, leading to entanglement and slower reaction kinetics.[12,16,17] However, above a critical salt concentration, competing factors (including chain branching) cause the viscosity to decrease with increasing salt. This behaviour forms one of the bases of industrial quality control systems that monitor and adjust the viscosity of product formulations.[2]

Most experimental efforts to study the properties of alkyl ethoxy sulphates have focused on commercial surfactants,[11,12,15] and characterisation studies of pure monodisperse solutions of SLE_nS are rare by comparison due to the challenges of synthesising and purifying the samples.[18–21] Experimental studies on the effect of the headgroup moieties have focused mainly on mixtures of otherwise polydisperse cationic/anionic, anionioc/nonionic and other surfactant combinations.[8,22–24] Meanwhile, recent developments in computational and molecular modelling studies[7,25–28] have focused on single-component analysis.

Given their wide array of applications ranging from personal care products to biomedical processes,[13,29,30] a rheological study of well-defined systems, ranging from pure systems to binary mixtures and multicomponent polydisperse solutions, is critical. In this work, a rheological study of solutions with 13 wt% surfactant concentration of different pure systems of SC_mE_nS and their mixtures is presented. This weight percent is chosen as a representative value for industrial formulations of typical consumer product surfactant systems, such as shampoo. A systematic analysis of the experimental rheological behaviour of a class of pure anionic surfactant formulations is presented, with a particular emphasis on understanding how the mean degree of ethoxylation and the mean alkyl tail length modulate the salt curve and rheology of the system.

2. Experimental

2.1. Reagents and synthesis of SC_mE_nS

Reagents and solvents are obtained from Sigma-Aldrich, Alfa Aesar and used without purification unless otherwise stated. Ultrapure water (18.2 MΩ cm at 20 °C) is used to prepare all formulations.

All SC_mE_nS molecules (except $SC_{12}E_0S$ and $SC_{16}E_0S$) are prepared based on three synthesis steps, which are exemplified in Fig. 1(b) for the case of $SC_{12}E_2S$. The steps for the synthesis are detailed in the ESI.†

2.2. Characterization of SC_mE_nS

The purity of the compounds is measured using ^{1}H and ^{13}C nuclear magnetic resonance (NMR) spectroscopy, mass spectrometry, and elemental analysis. NMR spectra are recorded at 25 °C using a 400 MHz spectrometer (Bruker AVANCE III HD nanobay, with a BBFO probe). Elemental analysis has been conducted on a Thermo Flash 2000. The complete characterisation data set is described in the ESI.†

2.3. Preparation of formulations

All formulations are prepared gravimetrically. The desired mass of each SC_mE_nS is measured in a sample vial followed by the addition of ultrapure water. This is then mixed with a vortex mixer until it is dissolved. Once dissolved, the required amount of sodium chloride is added through a 20% stock solution of NaCl in ultrapure water to achieve the correct weight concentrations of SC_mE_nS and NaCl. The resulting solution is then

mixed using a vortex mixer and stored at ambient temperature for 12 h to 48 h before rheology measurements. Evaporation is minimised by mixing and storing the formulations in an air-tight sample vial.

2.4. Rheology

Rheological measurements are performed on a TA HR10 rheometer with a cone and plate geometry (40 mm, 1.99417° cone angle, stainless steel) at 30 °C sampled at ten data points per decade. An oscillatory equilibration step is performed to ensure that the sample properties are in a steady state. Frequency sweeps are performed for f = 0.1 Hz to 100 Hz at 1% strain well within the linear viscoelastic regime. Steady shear sweeps are followed at shear rate values between 0.1 s^{-1} to 100 s^{-1}.

2.5. Numerical analysis of rheology

The zero-shear viscosity is obtained from the fittings of the Carreau-Yasuda[31] model to each steady shear measurement. Salt curves are constructed from the zero-shear viscosity and salt concentration per sample. Gaussian fits are then fitted to these salt curves to extract the key parameters at the peak. Additional thermodynamic quantities, specifically the scission energy E_{sc}, are obtained by fitting an extension to the Toy Shuffling model[12,17] to the oscillatory shear data. The model is only applied to points before the peak of the salt curve where wormlike micelles are known to be present.[16,17] A detailed workflow illustration is presented in the ESI† for more information.

3. Results and discussion

3.1. Behaviour of pure, monodisperse SLES

The experimental results for the salt curves of the monodisperse solutions of SLE_nS ($SC_{12}E_nS$) for different degrees of ethoxylation n of the head group are shown in Fig. 2, and include fittings of the experimental data to a Gaussian function. In this figure, an increase in the zero-shear viscosity η_0 is observed as the concentration of NaCl increases for all values of n studied until a viscosity peak is reached, followed by a decrease in the zero-shear viscosity with further addition of salt. The salt curves are observed to follow a nearly-perfect Gaussian shape that is often used in predictive modelling of the properties of surfactants.[11,12,15] The peak in the salt curve is a well-known effect driven by the topological changes of the self-assembled aggregates with increasing salt concentration,[2,3,11,15] which carries information on the morphological transition between long wormlike micelles to other more complex topologies, especially for ionic surfactants.[16,32] The position of the peak along the salt concentration c_s^{max}, which has been determined from the Gaussian fits, increases with the degree of ethoxylation, while the peak viscosity η_0^{max} follows the order: η_0^{max} = 73.6 Pa s at c_s^{max} = 6.1 wt% for n = 2, η_0^{max} = 55.9 Pa s at c_s^{max} = 5.0 wt% for n = 1, followed by η_0^{max} = 39.5 Pa s at c_s^{max} = 8.8 wt% for n = 3.

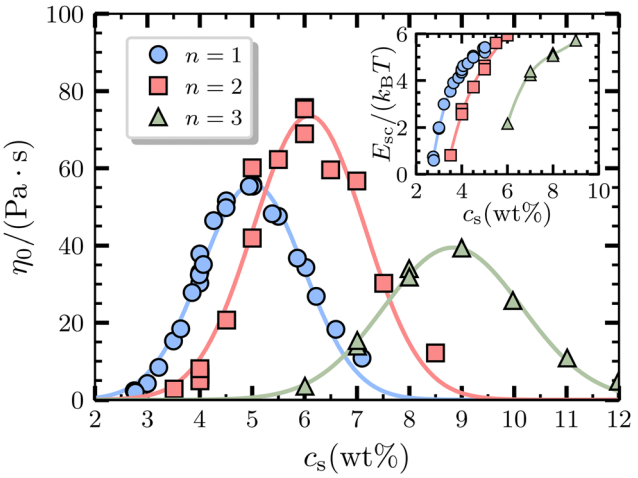

Fig. 2 Salt curves of pure monodisperse SLE_nS ($SC_{12}E_nS$) solutions for different degrees of ethoxylation n. The symbols correspond to the zero-shear viscosity η_0, obtained from fittings of the steady-shear measurement using the Carreau-Yasuda[31] model, as a function of salt (NaCl) concentration, c_s (wt%). The curves of the same color as the symbols correspond to the Gaussian curve fittings. (Inset) Results for the scission energy E_{sc} as a function of salt concentration c_s obtained from modeling the rheology of the solutions using the Toy Shuffling model[12,17] for salt concentrations before the peaks in the salt curves.

The results shown in Fig. 2 show that more salt is needed to reach peak viscosity as the length of the ethoxy linker increases. This trend suggests that the head-group architecture influences micellar assembly with ionic strength and could indicate the role of the ethoxylation moiety in the charge dispersion on the surface of micelles. Experimental and molecular simulations[26] have shown that the localisation/dispersion of counterions on the surface of the micelles formed by ionic surfactants drives the morphological transition. In the case of SDS, spheroids have localised concentrations of counterions from the additional electrolyte, while the cylindrical aggregates have more homogeneously dispersed counterions across the surface of the micelle.[26] For surfactants with extended headgroups, the ethoxy linkers tend to fold to remain close to the interface,[9] which could make the charges on the surface disperse even more.

This interaction between the ethoxy linker length and counterion dispersion effect could become more pronounced around the peak of the salt curve. To explain the change in microstructure with the salt concentration, it is necessary to discuss some geometrical aspects of micelle formation. The geometric constraints that describe the supramolecular structures that form and evolve in the solution can be mainly described by the packing parameter p, first introduced by Israelachvili.[3,33–35] The packing parameter is given by $p = V/(S_0R)$, where V and R are the volume and radius of the micelle core, respectively, being related to the length of the hydrocarbon tail, and S_0 is the area of the surface of the micelle hydrocarbon core at the oil–water interface.

A mechanism we propose to explain the pronounced counterion dispersion around the peak of the salt curve is that

longer ethoxy linkers disperse the charges more evenly, requiring more salt to create a uniform layer of counterions and reach the point of topological transition. This behaviour decreases the electrostatic repulsion between surfactant molecules and the interfacial tension, and as a consequence decreases the surface area S_0,[27] particularly for anionic alkyl ethoxy sulphated surfactants. This mechanism then promotes the formation of longer aggregates[8,20,27] at a salt concentration around the peak of the salt curve where longer micelles are present.[16,26,32]

The increase in the peak viscosity η_0^{max} from the degree of ethoxylation n = 1 to n = 2 could be due to the surfactant aggregates forming relatively bigger and longer micelles. The scission energy E_{sc} is well known to be closely related to the length of the wormlike micelles formed.[12,16,17,27] The inset of Fig. 2 shows a relative increase in scission energy E_{sc} around the salt curve peak, indicating the formation of longer micelles. The shift to a lower peak viscosity from n = 2 to n = 3 could therefore be explained by the formation of relatively smaller and shorter micelles inferred from the decrease in the scission energy shown in Fig. 2. Furthermore, in a recent study for similar systems using small-angle X-ray scattering (SAXS) experiments,[36] it has been reported that even at low salt concentrations, the aspect ratio of the microstructures formed by solutions of SLE_2S has a spherical cross section compared to the lower aspect ratios of SLE_1S or SLE_3S, which affects the packing in the structures formed in the presence of more counterions at high surfactant concentrations. An interplay between the hydrophilicity and flexibility of the headgroup as the number of ethoxy linkers increased could be involved in this trend.

Increasing the hydrophilic characteristics of the surfactant headgroup, which in this case is an increase in the ethoxy linker length, leads to changes in micelle formation and aggregate morphology based on the salt curves. An increase in the hydrophilic properties of the headgroup improves the dissolution of surfactants in the solvent, which promotes the formation of micelles of smaller size[7] and also reduces the critical micelle concentration (CMC)[18,37] for alkly ethoxy sulphates. Meanwhile, the decrease in scission energy E_{sc} is a factor that explains the formation of shorter micelles. This is also observed in molecular thermodynamic models[32] and dissipative particle dynamics (DPD) simulations for similar systems.[27] Another possible contributing factor is the effect of headgroup flexibility[9] on the dynamics of micellar structures, as extended ionic headgroups tend to fold back or remain close to the interface and modulate the local curvature. Furthermore, changes in the hydration state with salt concentration can influence the micelle dynamics. As the ionic headgroup becomes hydrated in both SDS[32] and SLE_nS,[36] the subsequent dehydration due to the increase in salt is expected to increase the repulsion in the headgroup to form shorter aggregates, hence the relatively lower E_{sc}, which is reflected macroscopically as a lower viscosity.

Molecular dynamics simulations of non-ionic surfactants[38,39] and amphiphilic colloidal dispersions[40] have shown a strong correlation between increased cluster aggregation number and increased bulk viscosity. In addition, in studies of non-ionic surfactants composed of units of k-ethylene oxide (EO) in the headgroup and alkyl chain in the tail, the increase in the number of EO units decreases the average aggregation number which could lead to a decrease in viscosity. This is shown for $k > 4$[41] and $k > 6$,[42] with k being the number of EO units. Experimental[19,21] and MD simulation[7] results have shown a trend in the aggregation number of pure SLE_nS samples similar to the trend in the change in the peak viscosities in this study.

To further investigate the trend in both peak viscosity and salt concentration, intermediate values of the degree of ethoxylation before and after the maximum observed at n = 2 are studied. In the next section, these systems are obtained by mixing two different surfactants that produce specific averages of the degree of ethoxylation $\bar{n}$.

3.2. Behaviour of binary mixtures of SC_mE_nS: effects of different tails and headgroups

Binary surfactant mixtures, with a total surfactant concentration ϕ_s = 13 wt%, have been used to systematically study the effect of different types of surfactants and compare their behaviour with respect to pure surfactant solutions. These binary mixtures are characterised by the weight-average ethoxilation number $\bar{n}$ and the weight-average alkyl tail length $\bar{m}$, defined as

$$\bar{x} = \frac{\sum_i \phi_i x_i}{\phi_s} \quad (1)$$

where ϕ_i is the weight fraction of the component i, and x is the degree of ethoxylation of the headgroup n or the length of the alkyl tail m. For each binary mixture, the viscosity η_0^{max} and salt concentration c_s^{max} at the peak of each salt curve are calculated to understand the effect of the components in the mixture.

First, to understand the effect of the different degrees of ethoxylation, keeping m = 12 constant, three sets of mixtures have been studied and correspond to: (a) binary mixtures of SLE_1S and SLE_nS, for n = [0, 2, 3], (b) binary mixtures of SLE_2S and SLE_nS, for n = [0, 3], and finally (c) binary mixtures of SLE_3S and SLE_0S. Note that SLE_0S corresponds to SDS. Any shifts in the salt concentration (c_s^{max}) and viscosity amplitude (η_0^{max}) at the peak of the salt curve in these mixtures are modulated by the increase in the proportion of the second component with respect to the first component. The results of the salt peaks for all these binary mixtures as a function of the average ethoxylation number $\bar{n}$, calculated using eqn (1), are presented in Fig. 3. In Fig. 3(a), it can be observed that the position of the salt peak c_s^{max} increases as the degree of ethoxylation n of the second SLE_nS component also increases, which mirrors the behaviour observed in the result of the pure components presented in Fig. 2. The results for the maximum viscosity of the salt peak η_0^{max} shown in Fig. 3(b) also mirror the behaviour observed in pure components, *i.e.*, the binary mixtures exhibit the largest values of η_0^{max} when the average ethoxylation number $\bar{n} \sim 2$.

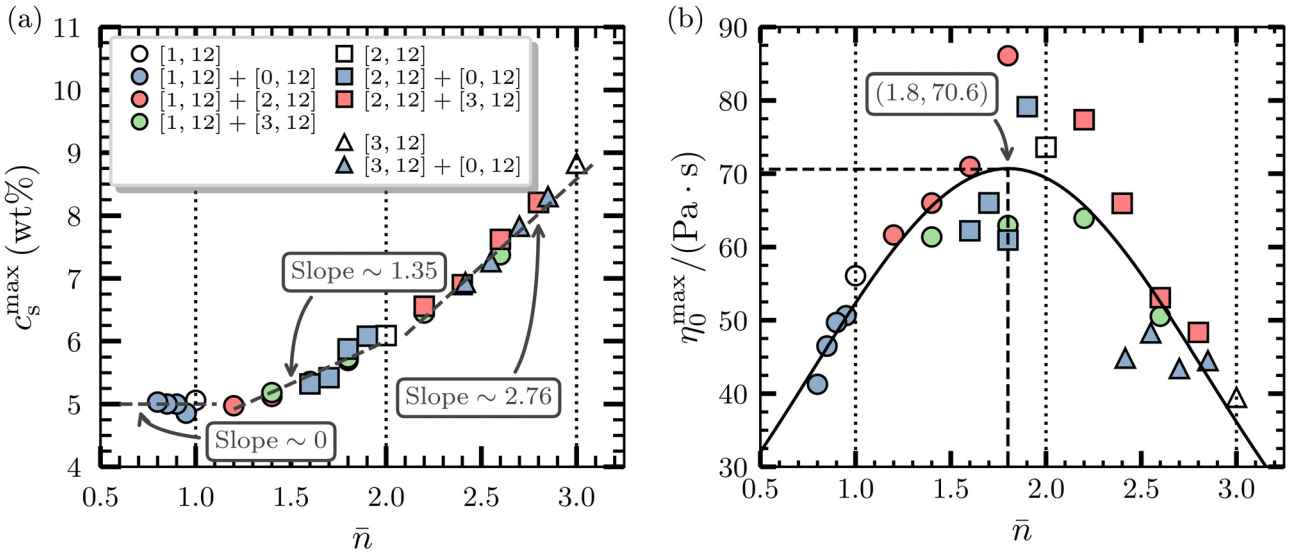

Fig. 3 Results for the (a) position of salt concetration c_s^{max} and (b) amplitude of the of the peak viscosity η_0^{max} of salt curves as a function of the average ethoxylation number $\bar{n}$ of binary mixtures of SLE$_n$S. The dashed lines in (a) indicate the slopes at which c_s^{max} increases as $\bar{n}$ increases. The continuous curve in (b) indicates the Gaussian fit of the data, with the position of the maximum of the curve indicated by the dashed lines. The dotted vertical lines in (a) and (b) indicate the location of the peaks for the pure monodisperse components.

For example, the addition of SLE$_2$S can be used if a formulation is required to have a higher viscosity, since this surfactant introduces more order, increasing the length of the micelles. Conversely, adding either SLE$_1$S or SLE$_3$S to a mixture generally reduces viscosity because these surfactants introduce entropy in the packing, which shortens the length of wormlike micelles.

This result is remarkable and indicates that a mixture of SLE$_n$S with an average ethoxylation number $\bar{n}$ exhibits a position of the peak similar to the pure component with the same ethoxylation number n, but with the advantage that the proportion of the components in the mixture can be tuned to target a specific viscosity. In other words, for predictions to determine the salt concentration at peak viscosity, one only needs knowledge of the average degree of ethoxylation and not the specific components in the solution.

In Fig. 3(a) one can also observe the development of three regimes in the position of the salt peak. First, the results indicate that the position of the salt peak remains constant at $c_s^{max} \sim 5$ for mixtures with $\bar{n} < 1$, which indicates that this is the minimum amount of salt needed to observe a peak in the salt curve for these systems and agrees with the position of the peak observed for pure SLE$_1$S. For the region $1 < \bar{n} < 2$, the position of the peak in the salt curve increases nearly linearly with a slope of $\sim$1.35, while for the region $2 < \bar{n} < 3$, the slope, at which c_s^{max} increases, doubles with respect to the previous regime. This remarkable observation allows us to modulate the amount of salt needed in a formulation to achieve a particular rheological behaviour by carefully choosing the ingredients. These findings could also have molecular and thermodynamic connections that are currently outside the experimental scope of this study but need to be explored. For example, the solvent-accessible surface area (SASA) per molecule for similar systems has been studied with molecular dynamics simulations by Wand *et al.*,[27] where it has been shown that increasing the salt concentration decreases the SASA, but increasing the ethoxy linker has the reverse effect. However, these trends have only been shown for single-component surfactant systems.

The peak viscosities shown in Fig. 3(b) appear to fall on a Gaussian curve with the position of the peak located close to the peak of pure SLE$_2$S. For single component solutions, the trend in the viscosity is consistent with the trends in aggregation numbers[19,21] and aspect ratios of micelles,[36] which peaks at ethoxy linker length $n = 2$ and lower values for $n = 1$ and $n = 3$. For binary surfactant systems, the trend appears to be modulated by the average length of the ethoxy linker. Thermodynamically, the maximum viscosity in a salt curve signals the imbalance in the chemical equilibrium between the cylinder and the endcap of a micelle, leading to a transition in topology.[26,32] At this transition point, the amount of salt needed to reach peak viscosity regardless of the components in a binary mixture implies that the surface area of the wormlike aggregates remains the same for any binary combination of surfactants. Viscosity has also been previously mentioned to be closely related to the aggregation number.[38,40] This could mean that an average ethoxy linker $n \approx 2$ forms the largest cluster aggregates, implying an order in the surfactant molecules that form the wormlike micelles. From MD simulation studies,[7,39,40] it has been shown that the shape of the cluster only serves as a secondary factor determining the viscosity. For binary surfactant systems, this could interact with self-recombination/non-self-recombination dynamics[17,38,39] due to the interaction of the component surfactant molecules. The effect could be due to the conformation and flexibility of the headgroup, the arrangement of the components, and the length of the micelle that affect the entropy and synergy in the packing, which changes the viscosity. These are open questions that will be the subject

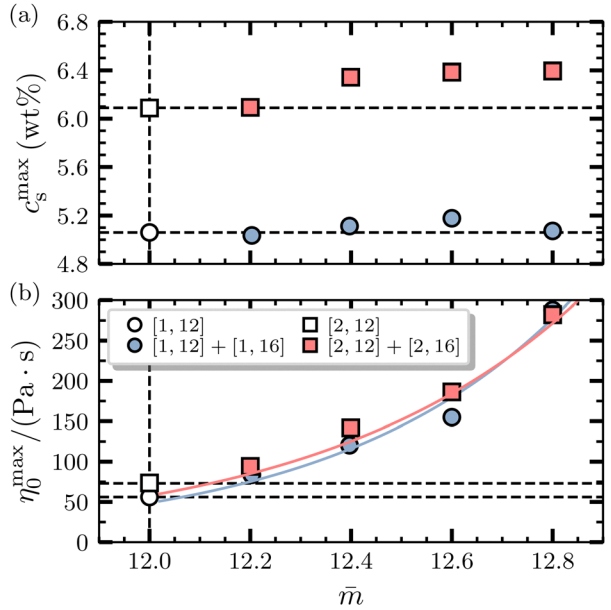

Fig. 4 Results for the (a) position of salt concentration c_s^{max} and (b) amplitude of the peak viscosity η_0^{max} of the salt curves as a function of the average alkyl tail length $\bar{m}$ of binary mixtures of SLE_nS and $SC_{16}E_nS$. The dashed lines indicate the positions of the peaks of the salt curves for pure SLE_nS, while the continuous curves in (b) are exponential fits.

of future studies for the anionic surfactant systems explored in this paper.

To observe changes in mixtures of different alkyl tail lengths, binary mixtures of surfactants with the same ethoxylation number n are used. These mixtures correspond to (a) SLE_1S and $SC_{16}E_1S$, and (b) SLE_2S and $SC_{16}E_2S$. The results for the salt position c_s^{max} and peak viscosity η_0^{max} of these binary mixtures as a function of the average alkyl tail length $\bar{m}$, calculated using eqn (1), are presented in Fig. 4. A slight increase in the position of the salt peak c_s^{max} is observed for the mixture with $n = 2$ as the average alkyl tail length increases in the mixture, with a plateau observed after $\bar{m}$ = 12.4. For mixtures with n = 1, a slight increase in the peak position is observed, but this is within the statistical error of the measurements. For both mixtures, on the contrary, the maximum viscosity η_0^{max} increases, almost exponentially, as $\bar{m}$ also increases, as can be seen from the exponential fittings in Fig. 4(b). For $\bar{m}$ = 12.8, the peak viscosity increases by approximately a factor of 5 for the mixture of SLE_1S and $SC_{16}E_1S$ when compared to pure SLE_1S, while the peak viscosity increases by approximately a factor of 4 for the mixture of SLE_2S and $SC_{16}E_2S$ when compared to pure SLE_2S. This behaviour can be attributed to the longer tail in $SC_{16}E_nS$, which increases the volume of the micelle core, forming larger aggregates. This behaviour is also observed in non-ionic surfactants and is well explained by thermodynamic models.[3,43] This increase in the viscosity also implies the formation of relatively longer micelles in the parts of the salt curve where wormlike micelles are expected. However, the increase in the volume of the micelle core has little effect on the salt concentration at the peak as discussed in Fig. 4(a) as electrostatic screening is influenced only by the charged headgroup and the changes in the electrolytes in solution.

3.3. Effect of ethoxylation polydispersity in mixtures of SLE_nS

Multicomponent mixtures of SLE_nS, with controlled degree of ethoxylation polydispersity, are studied to better understand the effect of ethoxy linkers in the headgroup on the rheology of solutions. These polydisperse mixtures are obtained combining four types of SLE_nS, corresponding to the values in n = [0, 1, 2, 3]. The degree of polydispersity is controlled by varying the amount of each component to achieve a specific variance around the mean ethoxylation number $\bar{n}$, which is defined as:

$$\text{Variance} = \frac{\sum_n (n-\bar{n})^2 \phi_n}{\sum_n \phi_n}, \qquad (2)$$

For this study, the polydisperse mixtures are designed to have mean ethoxylation numbers corresponding to $\bar{n}$ = 1.5,

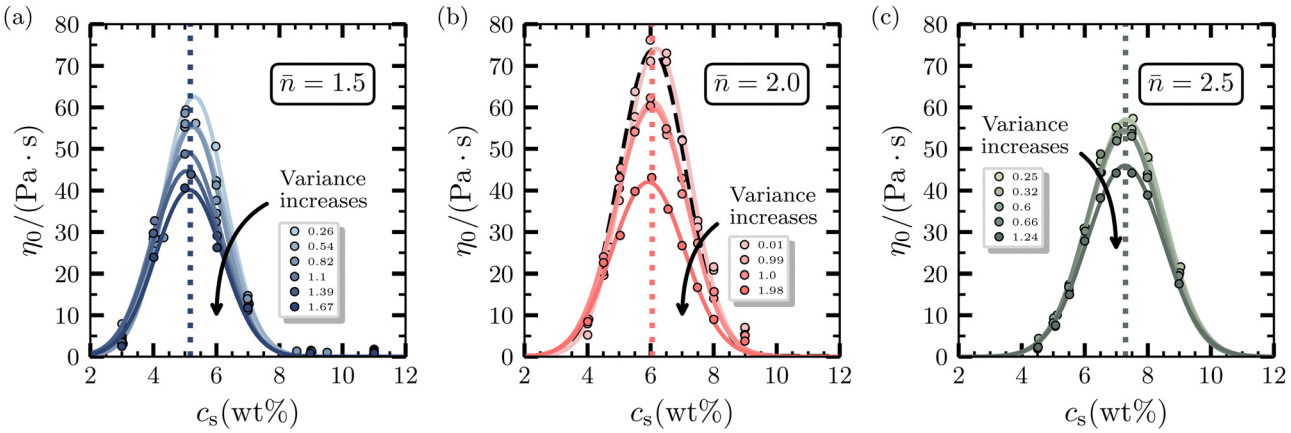

Fig. 5 Salt curves of multi-component mixtures of SLE_nS with average degree of ethoxylation $\bar{n}$ corresponding to (a) $\bar{n}$ = 1.5, (b) $\bar{n}$ = 2.0, and (c) $\bar{n}$ = 2.5. The circles correspond to the experimental values of the zero-shear viscosity η_0 as a function of salt (NaCl) concentration, c_s (wt%), while the curves corresponds to the Gaussian fits. The color shades of the curves from light to darker indicate an increase in the variance of the degree of ethoxylation. The vertical dotted lines indicate the average location of the salt-peak. The dashed curves in (b) correspond to the salt curve of pure monodisperse SLE_2S.

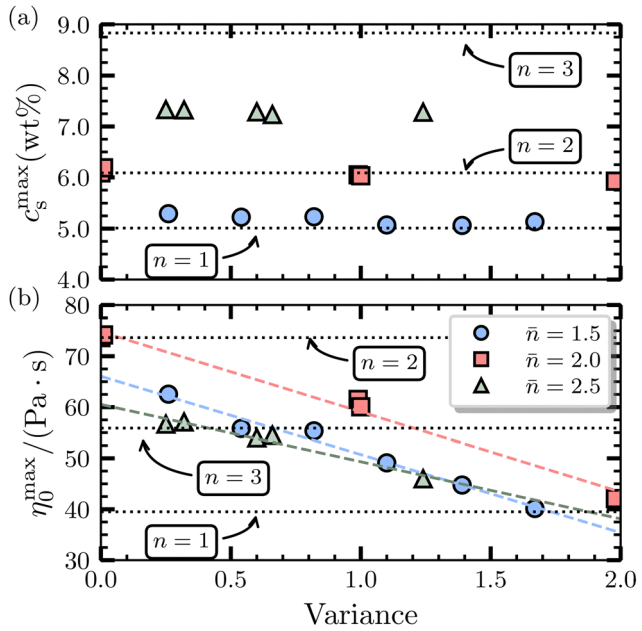

Fig. 6 Results for the (a) position c_s^{max} and (b) amplitude η_0^{max} of the peak viscosity of the salt curves as a function of the variance of the degree of ethoxylation in the mixtures of SLE_nS. The horizontal dotted lines indicate the peaks of the salt curves for pure monodisperse SLE_nS. The dashed lines in (b) are the linear fits of the peak viscosity.

$\bar{n}$ = 2.0, and $\bar{n}$ = 2.5, but keeping again the total surfactant concentration $\phi_s = \sum_n \phi_n$ at 13 wt%. The number of variance data points for each average ethoxylation value is limited by experimental and mixing constraints and is an area of potential exploration in terms of formulation space.

The results for the salt curves of the polydisperse systems for the three different average ethoxylation numbers $\bar{n}$ are presented in Fig. 5, with the change in the colour shades (from light to dark) in each set of symbols indicating an increase in the variance of the ethoxylation number of the mixtures. In Fig. 5, it is clear that for a given value of $\bar{n}$, all salt curves exhibit a peak located approximately at the same position regardless of the variance. The positions of these peaks correspond to c_s^{max} = 5.1 wt% for $\bar{n}$ = 1.5, c_s^{max} = 6.0 wt% for $\bar{n}$ = 2.0, and c_s^{max} = 7.3 wt% for $\bar{n}$ = 2.5, respectively. These results indicate that the position of the peak salt concentration c_s^{max} is independent of variations in the number of components in the mixture. This can also be observed later in Fig. 6(a) where the positions of the salt peaks are presented as a function of the variance. In Fig. 5(b), the salt curve for pure SLE_2S is also presented, which demonstrates how the polydisperse mixtures exhibit the same position of the peak as the pure, monodisperse solution with the same ethoxylation number.

In Fig. 5, it can be seen that the effect of having more than two headgroup moieties in the mixture is manifested only in the magnitude of the peak viscosity η_0^{max}. More specifically, it can be observed that the magnitude of the viscosity peak decreases as the variance of the mixture increases. This can also be observed in Fig. 6(b) where η_0^{max} is plotted against the variance of the mixture, and it is evident that the peak viscosity decreases almost linearly with the variance. The shape of the Gaussian curves fitted to the salt curves in Fig. 5 also remains qualitatively similar regardless of the polydispersity (variance) of the mixture.

The position of the peak salt concentration is independent of variations in the number of components in the mixture. Even when there are more than two types of headgroup moieties present in the micelles formed, the surface area of the wormlike micelles seems to be the same at the transition point. The consequence of maintaining the same surface area is in the packing of the micelles which affects the length observed as a change in viscosity. This is consistent with the previous observation made for binary mixtures where, for any combination of surfactant type in a mixture, the same amount of salt is needed to reach peak viscosity if the average degree of ethoxylation is the same.

4. Conclusions

This work presents a systematic study of the rheology and salt curves of pure single- and multicomponent systems of sodium alkyl ethoxy sulphates. Starting from the synthesis of well-defined pure components, binary and multicomponent mixtures of sodium alkyl ethoxy sulphates have been designed to study changes in the salt curves as a function of the degree of ethoxylation of the head group and the alkyl tail lengths. In particular, it has been demonstrated that increasing the length of the hydrocarbon tail increases the viscosity of the samples because of the increase in the volume of the micelle core. Furthermore, when there are more than two types of headgroup moiety in the mixture, the salt concentration to attain peak viscosity is modulated only by the average of the number of ethoxy linkers, while the peak viscosity is modulated by the relative proportion of the individual components present in the mixtures. The trends in the average ethoxylation and tail length reveal a Gaussian symmetry in the peak viscosity and regimes in the salt concentration needed to reach this peak. This also brings to light the macroscopic effects of headgroup flexibility when the ethoxy linkers are extended. The topological and dynamic properties of ionic surfactants are complex and additional experimental data are needed to fully elucidate these phenomena. However, the findings in this study provide the essential information needed for the design of new surfactants and the refinement of computational, molecular, and predictive models.

Conflicts of interest

There are no conflicts to declare.

Data availability

The data that support the findings of this study are available from the corresponding author(s) upon reasonable request.

Acknowledgements

The authors acknowledge financial support from an EPSRC Prosperity Partnership with Unilever: Center for Advanced Fluid Engineering and Digital Manufacturing (CAFE4DM) (Grant Reference No. EP/R00482X/1).

References

1 P. C. Hiemenz and R. Rajagopalan, *Principles of Colloid and Surface Chemistry*, CRC Press, 3rd edn, 1997.
2 K. Penfield, A. Co, G. L. Leal, R. H. Colby and A. J. Giacomin, *AIP Conf. Proc.*, 2008, **1027**, 899–901.
3 K. D. Danov, P. A. Kralchevsky, S. D. Stoyanov, J. L. Cook, I. P. Stott and E. G. Pelan, *Adv. Colloid Interface Sci.*, 2018, **256**, 1–22.
4 A. V. Shibaev, V. S. Molchanov and O. E. Philippova, *J. Phys. Chem. B*, 2015, **119**, 15938–15946.
5 O. SalahEldin Hussien, K. A. Elraies, A. Almansour, H. Husin, A. Belhaj and L. Ern, *J. Petrol. Sci. Eng.*, 2019, **183**, 106426.
6 B. Nikoobakht, Z. L. Wang and M. A. El-Sayed, *J. Phys. Chem. B*, 2000, **104**, 8635–8640.
7 S. D. Peroukidis, D. G. Mintis, I. Stott and V. G. Mavrantzas, *J. Phys. Mater.*, 2021, **4**, 044001.
8 L. Zhang, W. Kang, D. Xu, H. Feng, P. Zhang, Z. Li, Y. Lu and H. Wu, *RSC Adv.*, 2017, **7**, 13032–13040.
9 A. M. Forgiarini, C. Scorzza, J. Velásquez, F. Vejar, E. Zambrano and J. Salager, *J. Surfactants Deterg.*, 2010, **13**, 451–458.
10 M. Panoukidou, C. R. Wand, A. Del Regno, R. L. Anderson and P. Carbone, *J. Colloid Interface Sci.*, 2019, **557**, 34–44.
11 M. Pleines, W. Kunz, T. Zemb, D. Benczédi and W. Fieber, *J. Colloid Interface Sci.*, 2019, **537**, 682–693.
12 S. L. Flores, J. Mu, C. P. Cabry, J. Peterson, S. C. De Hert, L. Morrison, I. P. Stott, J. L. Cook, A. J. Masters, C. Hardacre and C. Avendaño, *J. Chem. Phys.*, 2023, **159**, 054902.
13 P. A. Cornwell, *Int. J. Cosmet. Sci.*, 2018, **40**, 16–30.
14 P. Fischer and H. Rehage, *Langmuir*, 1997, **13**, 7012–7020.
15 W. Fieber, A. Scheklaukov, W. Kunz, M. Pleines, D. Benczédi and T. Zemb, *J. Mol. Liq.*, 2021, **329**, 115523.
16 M. E. Cates and S. M. Fielding, *Adv. Phys.*, 2006, **55**, 799–879.
17 J. D. Peterson and M. E. Cates, *J. Rheol.*, 2021, **65**, 633–662.
18 M. Hato and K. Shinoda, *J. Phys. Chem.*, 1973, **77**, 378–381.
19 R. Triolo, E. Caponetti and V. Graziano, *J. Phys. Chem.*, 1985, **89**, 5743–5749.
20 C. Minero, E. Pramauro, E. Pelizzetti, V. Degiorgio and M. Corti, *J. Phys. Chem.*, 1986, **90**, 1620–1625.
21 S. E. Anachkov, K. D. Danov, E. S. Basheva, P. A. Kralchevsky and K. P. Ananthapadmanabhan, *Adv. Colloid Interface Sci.*, 2012, **183–184**, 55–67.
22 P. Pimenta and E. E. Pashkovski, *Langmuir*, 2006, **22**, 3980–3987.
23 C. Oelschlaeger, M. Schopferer, F. Scheffold and N. Willenbacher, *Langmuir*, 2009, **25**, 716–723.
24 L. Petrovic, J. Milinkovic, J. Fraj, S. Bucko, J. Katona and L. Spasojevic, *Colloid Polym. Sci.*, 2017, **295**, 2279–2285.
25 R. L. Anderson, D. J. Bray, A. Del Regno, M. A. Seaton, A. S. Ferrante and P. B. Warren, *J. Chem. Theory Comput.*, 2018, **14**, 2633–2643.
26 K. Schafer, H. B. Kolli, M. Killingmoe Christensen, S. L. Bore, G. Diezemann, J. Gauss, G. Milano, R. Lund and M. Cascella, *Angew. Chem., Int. Ed.*, 2020, **59**, 18591–18598.
27 C. R. Wand, M. Panoukidou, A. Del Regno, R. L. Anderson and P. Carbone, *Langmuir*, 2020, **36**, 12288–12298.
28 R. L. Hendrikse, A. E. Bayly and P. K. Jimack, *J. Phys. Chem. B*, 2022, **126**, 8058–8071.
29 I. Som, K. Bhatia and M. Yasir, *J. Pharm. BioAllied Sci.*, 2012, **4**, 2–9.
30 K. Stoyanova, Z. Vinarov and S. Tcholakova, *J. Drug Delivery Technol.*, 2016, **36**, 208–215.
31 K. Yasuda, PhD thesis, Massachusetts Institute of Technology, 1979.
32 K. D. Danov, P. A. Kralchevsky, R. D. Stanimirova, S. D. Stoyanov, J. L. Cook and I. P. Stott, *J. Colloid Interface Sci.*, 2021, **584**, 561–581.
33 J. N. Israelachvili, D. J. Mitchell and B. W. Ninham, *J. Chem. Soc., Faraday Trans. 2*, 1976, **72**, 1525.
34 J. N. Israelachvili, D. Mitchell and B. W. Ninham, *Biochim. Biophys. Acta*, 1977, **470**, 185–201.
35 J. N. Israelachvili, S. Marčelja and R. G. Horn, *Q. Rev. Biophys.*, 1980, **13**, 121–200.
36 A. P. Williams, J. M. Faber, C. Recsei, L. de Campo, T. A. Darwish, K. L. Tuck, R. R. Dagastine and R. F. Tabor, *J. Phys. Chem. B*, 2024, **128**, 6648–6653.
37 A. Del Regno, P. B. Warren, D. J. Bray and R. L. Anderson, *J. Phys. Chem. B*, 2021, **125**, 5983–5990.
38 Y. Koide and S. Goto, *J. Chem. Phys.*, 2022, **157**, 084903.
39 Y. Koide, *J. Chem. Phys.*, 2023, **159**, 224906.
40 Y. Kobayashi, N. Arai and A. Nikoubashman, *Soft Matter*, 2020, **16**, 476–486.
41 S. Puvvada and D. Blankschtein, *J. Chem. Phys.*, 1990, **92**, 3710–3724.
42 R. Nagarajan and E. Ruckenstein, *Langmuir*, 1991, **7**, 2934–2969.
43 K. D. Danov, P. A. Kralchevsky, S. D. Stoyanov, J. L. Cook and I. P. Stott, *J. Colloid Interface Sci.*, 2019, **551**, 227–241.